

Four Easy Pieces

Carl M Bender

Department of Physics, Washington University, St. Louis MO 63130, USA

Abstract. This paper is a mini-summary of four new advances in the theory of \mathcal{PT} -symmetric quantum mechanics. It describes some new calculations that were completed in 2005. The first advance concerns the classical coordinate-space trajectories in some \mathcal{PT} -symmetric theories. Depending on the initial conditions, one can find arbitrarily long periodic \mathcal{PT} -symmetric classical trajectories. The longer trajectories originate from smaller regions of initial conditions. There is an interesting resemblance to the so-called period-doubling route to chaos. The second advance concerns the perturbative construction of the \mathcal{C} operator for a \mathcal{PT} -symmetric square well. The result has notable similarities to and differences from that for the \mathcal{PT} -symmetric cubic oscillator. The third advance is a detailed comparison of a \mathcal{PT} -symmetric Hamiltonian and the corresponding Hermitian Hamiltonian. It is argued that a perturbative construction of the Hermitian Hamiltonian leads to an almost intractable theory. The fourth advance concerns reflectionless potentials and \mathcal{PT} symmetry and a possible connection with problems in cosmology.

Submitted to: *J. Phys. A: Math. Gen.*

PACS numbers: 11.30.Er, 45.50.Dd, 02.30.Fn

1. Introduction

The purpose of this paper is to summarize four very recent developments in the study of \mathcal{PT} -symmetric Hamiltonians. The first concerns a detailed study in collaboration with Chen, Darg, and Milton of classical \mathcal{PT} -symmetric Hamiltonians [1]. The focus of this study is on the class of Hamiltonians

$$H = p^2 + x^2(ix)^\epsilon \quad (\epsilon \geq 0). \quad (1)$$

Hamiltonians of this form were first introduced in Ref. [2]. This is a large class of complex \mathcal{PT} -symmetric non-Hermitian quantum-mechanical Hamiltonians whose spectra are real [3] and which exhibit unitary time evolution [4]. What is the nature of the underlying classical theories described by these Hamiltonians? The first study of the classical mechanics of these Hamiltonians was done in 1999 [3] and a more recent study was published in 2004 [4]. While these studies reported a number of interesting results, many remarkable features of the classical trajectories were not discovered. We report in Sec. 2 some new and surprising properties of classical orbits.

The second topic addressed here concerns the \mathcal{C} operator for the \mathcal{PT} -symmetric square well. A quantum-mechanical Hamiltonian having an unbroken \mathcal{PT} symmetry also possesses a hidden symmetry that is represented by the linear operator \mathcal{C} [4]. This symmetry operator \mathcal{C} guarantees that the Hamiltonian acts on a Hilbert space with an inner product that is both positive definite and conserved in time, thereby ensuring that the Hamiltonian can be used to define a unitary theory of quantum mechanics. In Sec. 3 it is shown how to construct the operator \mathcal{C} for the \mathcal{PT} -symmetric square well using perturbative techniques. The results discovered in collaboration with Tan [7] are somewhat surprising because the \mathcal{C} operator, even for this elementary potential, is found to have a new and rather complicated structure.

The third topic involves work done in collaboration with Chen and Milton [8] regarding the relationship between a \mathcal{PT} -symmetric Hamiltonian H and the corresponding Hermitian Hamiltonian h . Section 4 compares both forms of a non-Hermitian ix^3 quantum-mechanical Hamiltonian and demonstrates that it is much harder to perform calculations in the Hermitian theory because the perturbation series for the Hermitian Hamiltonian is constructed from divergent Feynman graphs.

Finally, in Sec. 5 we review recent work done in collaboration with Ahmed and Berry [9]. The point of this work is that the eigenvalues of a \mathcal{PT} -symmetric $-x^4$ potential can be obtained without having to impose boundary conditions in the complex- x plane. The boundary conditions on the real- x axis are simply that the potential be reflectionless. This work suggests some interesting possible applications in cosmological models.

2. Classical Trajectories for \mathcal{PT} -Symmetric Hamiltonians

The possible trajectories $x(t)$ for a classical particle whose dynamics is governed by the Hamiltonian (1) have a rich and elaborate structure that depends sensitively on the initial conditions. Without loss of generality we may assume that the energy of a classical particle is 1, and we can solve numerically the Heisenberg equations of motion.

Three interesting features of these trajectories were discovered in previous studies [5, 6]: First, a complex non-Hermitian Hamiltonian typically generates complex classical trajectories. Thus, even if the classical particle is initially on the real- x axis, it is subject to complex forces and thus to obey the complex version of Newton's third law it will move off the real axis and travel through the complex plane. For example, in Fig. 1 we display three closed classical trajectories for the case $\epsilon = \pi - 2$. First, there is the path connecting the turning points, which which are indicated by dots. Two other trajectories that enclose these two turning points are also indicated.

When $\epsilon = 0$ there are two turning points on the real- x axis, but as ϵ increases from 0, this pair of turning points at $x = \pm 1$ moves downward into the complex- x plane. These turning points are determined by the equation $1 + (ix)^{2+\epsilon} = 0$. When ϵ is noninteger, this equation has many solutions, all having absolute value 1: $x = \exp\left(i\pi \frac{4N-4-\epsilon}{4+2\epsilon}\right)$, where N is an integer. These turning points occur in \mathcal{PT} -symmetric pairs (that is, pairs that are reflected through the imaginary axis) labeled by $k = 1, 2, 3, \dots$. For each k the pair

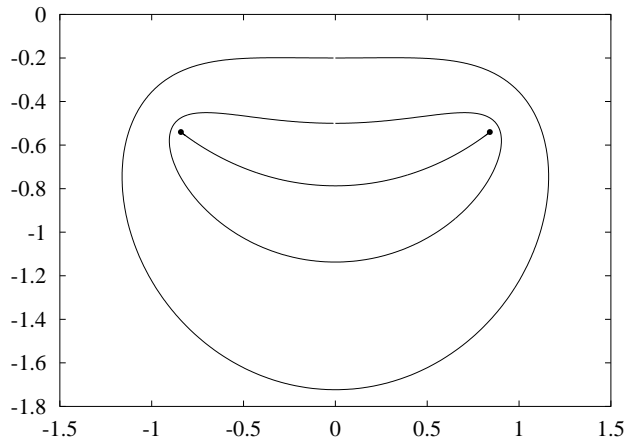


Figure 1. Classical trajectories in the complex- x plane for the complex oscillator whose Hamiltonian $H = p^2 - (ix)^\pi$ is obtained by setting $\epsilon = \pi - 2$ in (1). The trajectories represent possible paths of a classical particle. By virtue of Cauchy's integral theorem all closed trajectories have the same period T as given in (2).

of turning points is given by $N = k$ and $N = -k + 1$. Note that the pair of turning points at $\epsilon = 0$ deforms continuously into the $k = 1$ pair of turning points when $\epsilon \neq 0$. For $\epsilon = \pi - 2$ these turning points are shown in Fig. 1 as dots.

The general formula for the period of a closed orbit whose topology is like that of the orbits shown in Fig. 1 is [5]

$$T = 2\sqrt{\pi} \frac{\Gamma\left(\frac{3+\epsilon}{2+\epsilon}\right)}{\Gamma\left(\frac{4+\epsilon}{4+2\epsilon}\right)} \cos\left(\frac{\epsilon\pi}{4+2\epsilon}\right) \quad (\epsilon \geq 0). \quad (2)$$

For the closed orbits shown in Fig. 1, we find that $T = 2.33276$.

A second previously known feature of the classical trajectories is that the classical domain for the Hamiltonian (1) is a multisheeted Riemann surface when ϵ is noninteger. Thus, the classical trajectory may visit more than one sheet of the Riemann surface. In Ref. [5] classical trajectories that visit three sheets of the Riemann surface were discovered, but no trajectories were found that entered more than three sheets. To construct closed orbits having a more complicated topological structure than those shown in Fig. 1, we take $\epsilon = \pi - 2$ and choose an initial condition for which the classical trajectory crosses the branch cut on the positive imaginary axis and leaves the principal sheet of the Riemann surface. In Fig. 2 we show such a trajectory. This trajectory visits three sheets of the Riemann surface, the principal sheet (sheet 0) on which the trajectory is shown as a solid line, and sheets ± 1 on which the trajectory is shown as a dashed line. On the Riemann surface the resulting trajectory is \mathcal{PT} -symmetric (left-right symmetric). The period of the orbit in Fig. 2 is $T = 11.8036$, which is roughly five times longer than the periods of the orbits shown in Fig. 1. This is because the orbit is topologically more complicated and encloses branch cuts joining three pairs rather than one pair of complex turning points. (The period of the orbit is roughly proportional to the number of times that the orbit crosses the imaginary axis.)

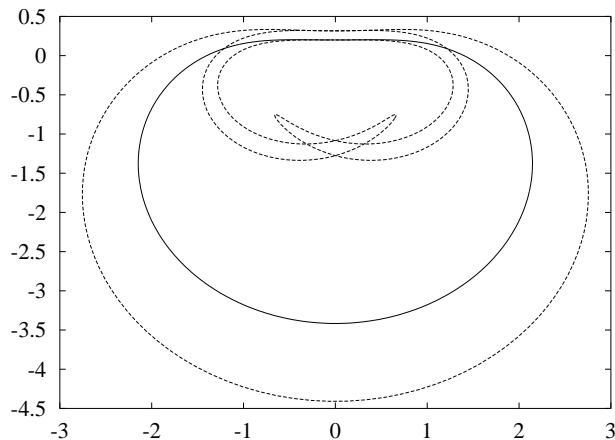


Figure 2. A classical trajectory in the complex- x plane for the Hamiltonian $H = p^2 - (ix)^\pi$. The initial condition is chosen so that the path crosses the branch cut on the positive imaginary axis and leaves the principal sheet of the Riemann surface. On the principal sheet the trajectory is indicated by a solid line. The classical particle visits two other sheets of the Riemann surface on which the trajectory is indicated by a dashed line. The closed orbit is \mathcal{PT} symmetric (has left-right symmetry).

A third previously known feature of the classical trajectories is that the classical trajectories manifest the \mathcal{PT} symmetry of the Hamiltonian. Under parity reflection \mathcal{P} the position of the particle changes sign: $\mathcal{P} : x(t) \rightarrow -x(t)$. Under time reversal \mathcal{T} the sign of both t and i are reversed, so $\mathcal{T} : x(t) \rightarrow x^*(-t)$. Thus, under combined \mathcal{PT} reflection the classical trajectory is replaced by its mirror image with respect to the imaginary axis on the principal sheet of the Riemann surface. When $\epsilon \geq 0$, the \mathcal{PT} symmetry of H in (1) at the quantum level is unbroken and, as a consequence, the classical orbits are closed periodic paths in the complex plane. When ϵ is negative, the classical trajectories are open (and nonperiodic). In Fig. 3 we consider the case $\epsilon = -0.2$ and show a pair of paths that begin on the negative imaginary axis. One path evolves forward in time and the other path evolves backward in time. Each path spirals outward and eventually moves off to infinity. Note that the pair of paths is a \mathcal{PT} -symmetric structure. Note also that the paths do not cross because they are on different sheets of the Riemann surface. The function $(ix)^{-0.2}$ requires a branch cut, and we take this branch cut to lie along the positive imaginary axis. The forward-evolving path leaves the principal sheet (sheet 0) of the Riemann surface and crosses the branch cut in the positive sense and continues on sheet 1. The reverse path crosses the branch cut in the negative sense and continues on sheet -1 . Figure 3 shows the projection of the classical orbit onto the principal sheet.

We have recently discovered that the structure of the complex trajectories is much richer and more elaborate than previously noticed. One can find trajectories that visit huge numbers of sheets of the Riemann surface and exhibit fine structure that is exquisitely sensitive to the initial condition $x(0)$ and to the value of ϵ . Small variations in $x(0)$ and ϵ give rise to dramatic changes in the topology of the classical orbits and to

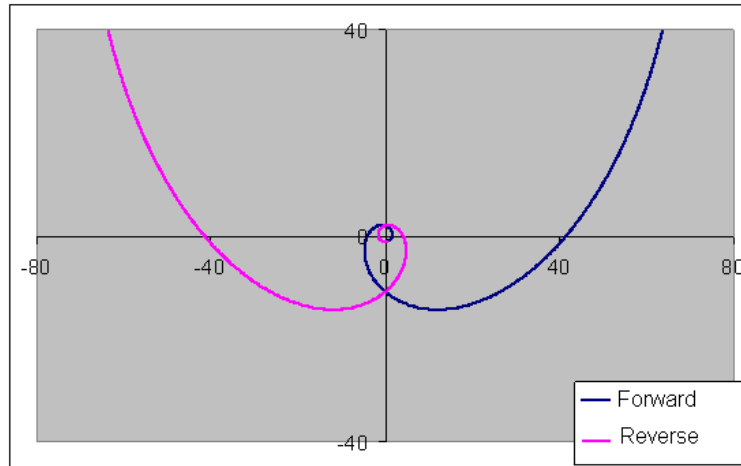


Figure 3. Classical trajectories in the complex- x for the Hamiltonian in (1) with $\epsilon = -0.2$. These trajectories begin on the negative imaginary axis very close to the origin. One trajectory evolves forward in time and the other goes backward in time. The trajectories are open orbits and show the particle spiraling off to infinity. The trajectories begin on the principal sheet of the Riemann surface; as they cross the branch cut on the positive imaginary axis, they visit the higher and lower sheets of the surface. Note that the trajectories do not cross because they lie on different sheets.

the size of the period. Depending on the value of $x(0)$, there are periodic orbits having short periods as well as orbits having very long and possibly infinitely long periods. These results are reminiscent of the period-lengthening route to chaos that is observed in logistic maps. Furthermore, for a given initial condition the classical behavior undergoes remarkable transitions as ϵ is varied. This behavior is described in detail in Ref. [1]. We focus here on the dependence of classical orbits on initial conditions.

We have found initial conditions that generate trajectories that visit many sheets repeatedly. Figure 4 shows a classical trajectory starting at $x(0) = -7.1i$ that visits 11 sheets of the Riemann surface. Its period is $T = 255.3$. The structure of this orbit near the origin is complicated and thus a magnified version is shown in Fig. 5. Figures 4 and 5 are complicated, so we give a more understandable representation of the classical orbit in which we plot the complex phase (argument) of $x(t)$ as a function of t . In Fig. 6 we present such a plot showing the complex phase for one full period.

The period of the classical orbits is exquisitely sensitive to the initial conditions. To illustrate this sensitivity we show in Fig. 7 the size of the period for $\epsilon = \pi - 2$ as a function of the initial condition $x(0)$ in a small portion of the complex- x plane containing the negative imaginary axis from $-8.5i$ to $-9.0i$. Note that initial conditions chosen from this small region give rise to classical orbits whose periods range from 231.1 up to 28,104.7. The regions of extremely long periods become narrower and more difficult to observe numerically. It is impossible to resolve the fine detail between the two longest periods, and we conjecture that there are infinitely many arbitrarily thin regions of initial conditions between $-8.767i$ and $-8.770i$ that give rise to arbitrarily long periods.

We display in Fig. 8 one of the long-period orbits in Fig. 7. Figure 8 shows the

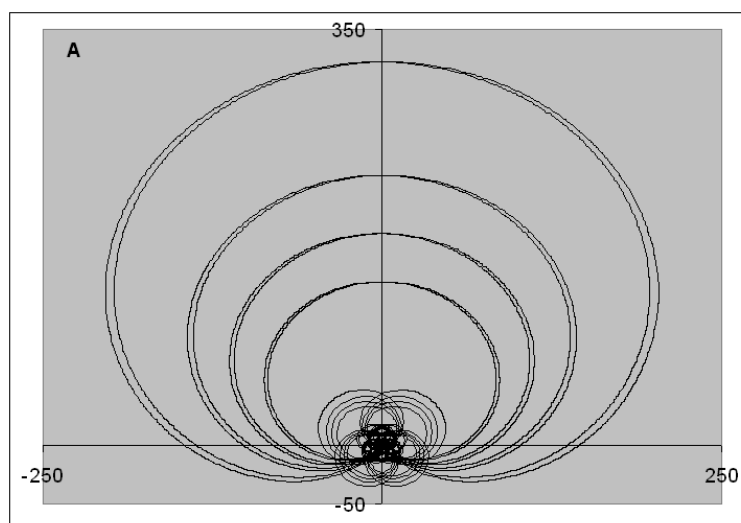


Figure 4. A classical trajectory in the complex- x plane for the complex Hamiltonian $H = p^2 - (ix)^\pi$. This complicated trajectory begins at $x(0) = -7.1i$ and visits 11 sheets of the Riemann surface. Its period is approximately $T = 255.3$. This figure displays the projection of the trajectory onto the principal sheet of the Riemann surface. Note that this trajectory does not cross itself.

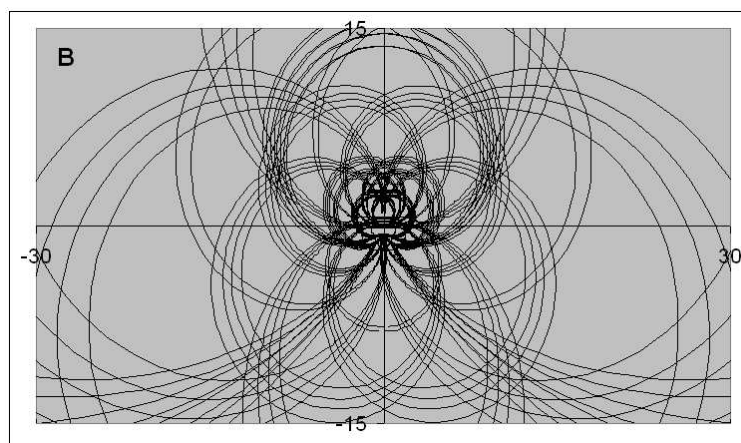


Figure 5. An enlargement of the classical trajectory $x(t)$ in Fig. 4 showing the detail near the origin in the complex- x plane. This classical path never crosses itself; the apparent self-intersections are paths on different sheets of the Riemann surface.

complex argument of $x(t)$ as a function of time t for $\epsilon = \pi - 2$ and initial condition $x(0) = -8.63026i$. This orbit has period $T = 10,554.9$ and visits 17 sheets of the Riemann surface. The inset displays the fine structure of this oscillatory behavior.

A characteristic feature of long orbits is the persistent oscillation in the classical path. There are huge numbers of concentric U-turns in portions of the complex plane. These U-turns focus about one of the many complex turning points and illustrate in a rather dramatic fashion the complex nature of the classical turning point. In Fig. 9 we plot the complex argument of $x(t)$ as a function of time t for $\epsilon = \pi - 2$ and initial condition $x(0) = -17i$. This orbit has period $T = 452.6$ and visits 5 sheets of the

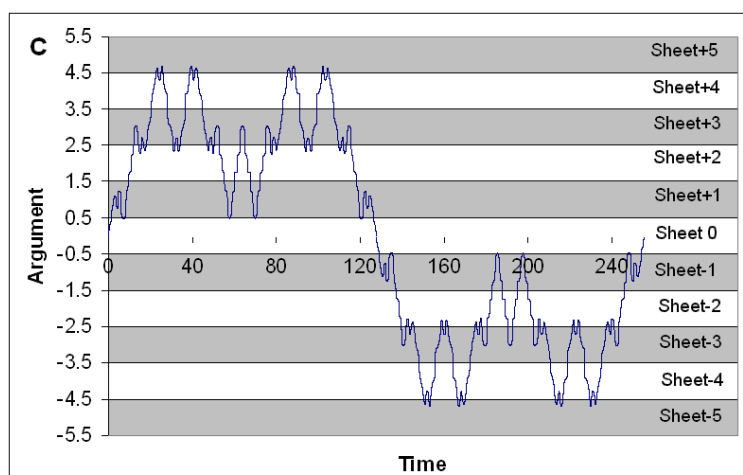


Figure 6. Argument (complex phase) of the classical orbit shown in Figs. 4 and 5 plotted as a function of time for one complete cycle. The period of this cycle is $T = 255.3$. The classical particle starts on the negative imaginary axis on sheet 0 where the phase is defined to be 0. The particle then visits 11 sheets of the Riemann surface from sheet -5 to sheet 5 before returning to its starting point.

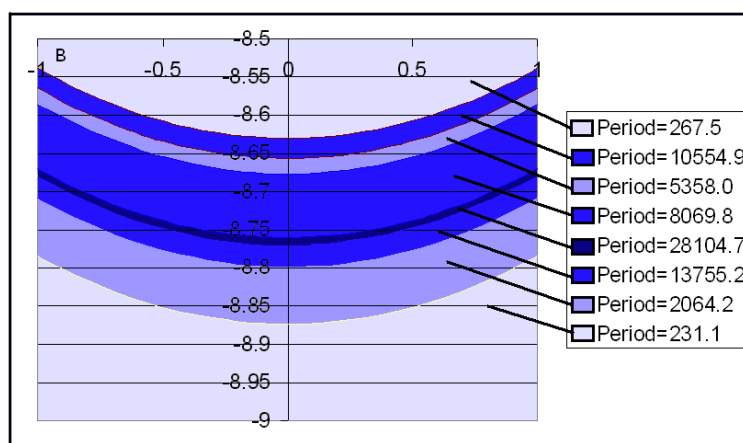


Figure 7. Small portion of the complex- x plane showing the dependence of the periods T of the classical orbits on the choice of initial condition $x(0)$ for the case $\epsilon = \pi - 2$. Note that T is extremely sensitive to the value of $x(0)$. There is an unresolved region between the band corresponding to $T = 28,104.7$ and $T = 13,755.2$. We conjecture that arbitrarily long periods can be found in arbitrarily thin regions between $x(0) = -8.767i$ and $x(0) = -8.770i$.

Riemann surface. We show the U-turns of this orbit near a turning point in Fig. 10.

Figures 9 and 10 explain heuristically how very long-period orbits arise. For a classical trajectory to travel a great distance in the complex plane, its path must weave through a mine field of turning points. If the trajectory comes under the influence of a distant turning point, it executes a large number of concentric U-turns and is eventually thrown back to its starting point. However, if the initial condition is chosen carefully, the complex trajectory can weave past many turning points before it eventually encounters

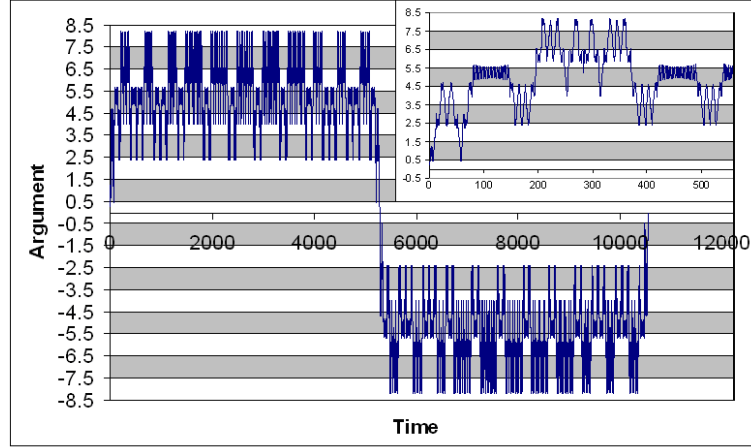


Figure 8. Argument of a long-period classical orbit for which $\epsilon = \pi - 2$ and the initial condition is $x(0) = -8.63026i$. This orbit has period $T = 10,554.9$ and visits 17 sheets of the Riemann surface. The inset shows the fine oscillatory structure.

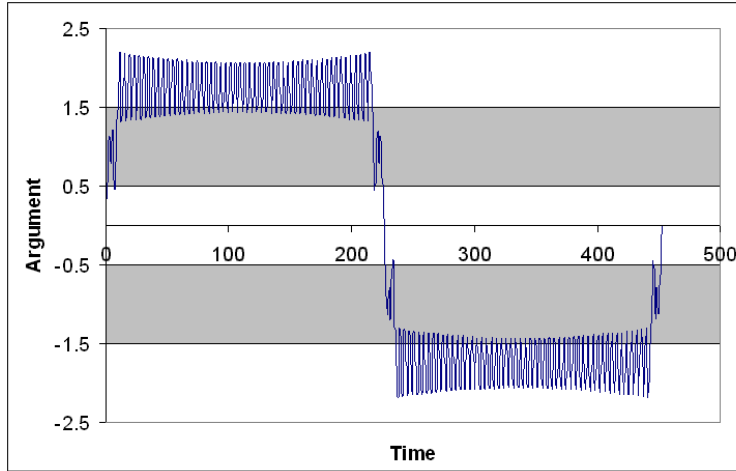


Figure 9. Argument of the classical orbit as a function of time t for $\epsilon = \pi - 2$ and initial condition $x(0) = -17i$. This orbit has period $T = 452.6$ and visits 5 sheets of the Riemann surface. Note the persistent oscillation in the classical orbit.

a turning point that takes control of the classical particle. We speculate that it may be possible to find a special critical initial condition for which the classical path manages to avoid and weave past all turning points and therefore has an infinitely long period.

3. The \mathcal{C} Operator for the \mathcal{PT} -Symmetric Square Well

An especially simple and elegant model of a quantum-mechanical Hamiltonian having an unbroken \mathcal{PT} -symmetry is the \mathcal{PT} -symmetric square well, whose Hamiltonian $H = p^2 + V(x)$ has the potential $V(x) = \infty$ for $x < 0$ and $x > \pi$ and

$$V(x) = \begin{cases} i\epsilon & \text{for } \frac{\pi}{2} < x < \pi, \\ -i\epsilon & \text{for } 0 < x < \frac{\pi}{2}. \end{cases} \quad (3)$$

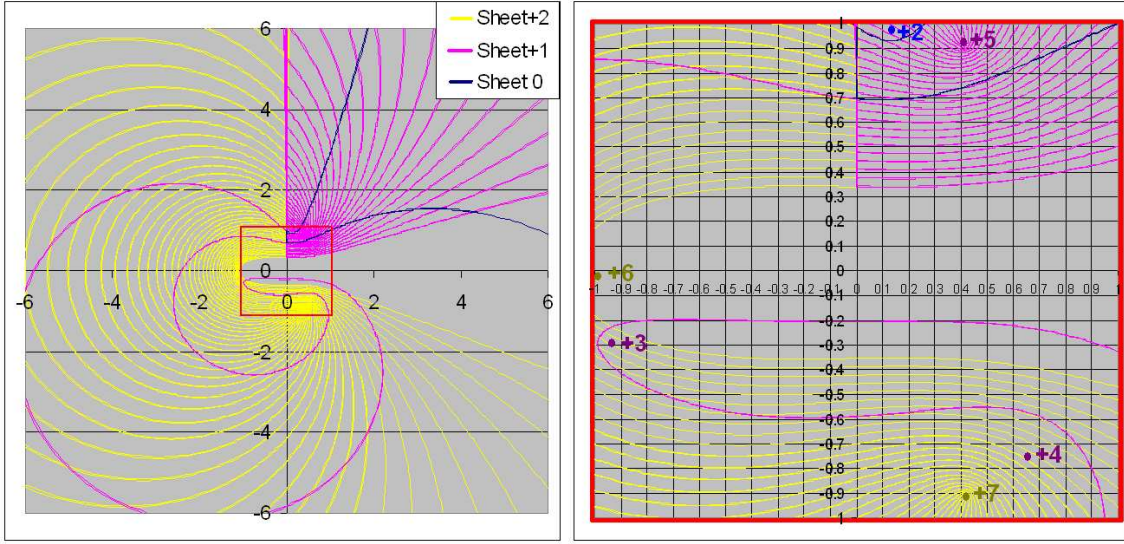


Figure 10. Classical orbit in the complex- x plane corresponding to Fig. 9. The oscillation in Fig. 9 corresponds to concentric U-turns around a complex turning point.

This Hamiltonian reduces to the conventional Hermitian square well in the limit $\epsilon \rightarrow 0$. For this H the parity operator \mathcal{P} performs a reflection about $x = \frac{\pi}{2}$: $\mathcal{P} : x \rightarrow \pi - x$. The \mathcal{PT} -symmetric square-well Hamiltonian was invented and first examined by Znojil [10] and it has been heavily studied by many other researchers [11].

To interpret a non-Hermitian \mathcal{PT} -symmetric Hamiltonian as defining a conventional quantum-mechanical model it is necessary to find the hidden symmetry operator \mathcal{C} . This operator is used to define the Hilbert-space inner product with respect to which the Hamiltonian H is self-adjoint [4]. In Ref. [4] the \mathcal{C} operator in coordinate space was shown to have a representation as a sum over the eigenfunctions $\phi_n(x)$ of H :

$$\mathcal{C}(x, y) = \sum_{n=0}^{\infty} \phi_n(x) \phi_n(y). \quad (4)$$

The eigenfunctions are normalized to be eigenstates of \mathcal{PT} with eigenvalue 1,

$$\mathcal{PT} \phi_n(x) = \phi_n(x), \quad (5)$$

and the integral of the square of the n th eigenfunction oscillates in sign:

$$\int dx [\phi_n(x)]^2 = (-1)^n. \quad (6)$$

For complicated Hamiltonians the \mathcal{C} operator cannot be obtained in closed form. However, Ref. [12] explains how to evaluate perturbatively the sum in (4) for the Hamiltonian

$$H = p^2 + x^2 + i\epsilon x^3. \quad (7)$$

In Ref. [13] the methods used in Refs. [12] were extended to systems having an infinite number of degrees of freedom. It was shown how to solve the three simultaneous algebraic equations satisfied by \mathcal{C} :

$$\mathcal{C}^2 = 1, \quad [\mathcal{C}, \mathcal{PT}] = 0, \quad [\mathcal{C}, H] = 0. \quad (8)$$

In Ref. [13] the \mathcal{C} operator is demonstrated to be a product of the exponential of an antisymmetric Hermitian operator Q and the parity operator \mathcal{P} :

$$\mathcal{C} = e^Q \mathcal{P}. \quad (9)$$

In all the examples studied so far the \mathcal{C} operator is a combination of integer powers of x and integer numbers of derivatives multiplying the parity operator \mathcal{P} . Hence, the Q operator is a polynomial in the operators x and $p = -i\frac{d}{dx}$. The novelty of the \mathcal{PT} -symmetric square-well potential (3) is that \mathcal{C} contains *integrals* of \mathcal{P} and thus the Q operator, while it is a simple function, is *not* a polynomial in x and p . Therefore, it cannot be found easily by the algebraic perturbative methods introduced in Ref. [13].

Our procedure here is first to solve the Schrödinger equation

$$-\phi_n''(x) + V(x)\phi_n(x) = E_n\phi_n(x) \quad (n = 0, 1, 2, 3, \dots) \quad (10)$$

subject to the boundary conditions $\phi_n(0) = \phi_n(\pi) = 0$. We obtain $\phi_n(x)$ as a perturbation series to second order in powers of ϵ . The eigenfunctions are normalized according to (5) and (6). Then, we evaluate the sum in (4). The advantage of the domain of the square well being $0 < x < \pi$ is that this sum reduces to Fourier sine and cosine series that can be summed exactly. After evaluating the sum, we translate the domain of the square well to the symmetric region $-\frac{\pi}{2} < x < \frac{\pi}{2}$. On this domain the parity operator in coordinate space is $\mathcal{P}(x, y) = \delta(x + y)$. Finally, we show that the \mathcal{C} operator to order ϵ^2 has the form in (9), and we evaluate Q to order ϵ^2 .

We begin by solving the Schrödinger equation (10) in the right ($x > \frac{\pi}{2}$) and left ($x < \frac{\pi}{2}$) regions of the square well:

$$\begin{aligned} \phi_{n,R}(x) = a_n & \left\{ i^{\frac{1}{2}(1-(-1)^n)} \sin(n+1)x \right. \\ & + \left[i^{\frac{1}{2}(1+(-1)^n)} \left(\frac{\pi-x}{2} \right) \frac{(-1)^n \cos(n+1)x}{(n+1)} - \frac{1}{2}(1-(-1)^n) \frac{\sin(n+1)x}{2(n+1)^2} \right] \epsilon \\ & + i^{\frac{1}{2}(1-(-1)^n)} \left[\frac{1}{2}(1+(-1)^n) \left(\frac{x-\pi}{4} \right) \frac{\cos(n+1)x}{(n+1)^3} + \left(\frac{x^2}{8} - \frac{\pi x}{4} + \frac{\pi^2}{16} \right) \frac{\sin(n+1)x}{(n+1)^2} \right] \epsilon^2 \\ & \left. + \mathcal{O}(\epsilon^3) \right\} \quad (x > \frac{\pi}{2}), \end{aligned} \quad (11)$$

$$\begin{aligned} \phi_{n,L}(x) = a_n & \left\{ i^{\frac{1}{2}(1-(-1)^n)} \sin(n+1)x \right. \\ & + \left[i^{\frac{1}{2}(1+(-1)^n)} \frac{x}{2} \frac{(-1)^n \cos(n+1)x}{(n+1)} + \frac{1}{2}(1-(-1)^n) \frac{\sin(n+1)x}{2(n+1)^2} \right] \epsilon \\ & + i^{\frac{1}{2}(1-(-1)^n)} \left[\frac{1}{2}(1+(-1)^n) \frac{x \cos(n+1)x}{4(n+1)^3} + \left(\frac{x^2}{8} - \frac{\pi^2}{16} \right) \frac{\sin(n+1)x}{(n+1)^2} \right] \epsilon^2 \\ & \left. + \mathcal{O}(\epsilon^3) \right\} \quad (x < \frac{\pi}{2}). \end{aligned} \quad (12)$$

These eigenfunctions and their first derivatives are continuous at $x = \frac{\pi}{2}$. Next, we impose the normalization requirements in (5-6) to find the coefficient a_n in (11) - (12):

$$a_n = \sqrt{\frac{2}{\pi}} \left[1 - (-1)^n \left(\frac{(2 - (-1)^n)}{(6 - 2(-1)^n)(n+1)^4} - \frac{(-1)^n \pi^2}{16(n+1)^2} \right) \epsilon^2 + \mathcal{O}(\epsilon^4) \right]. \quad (13)$$

With this normalization, the \mathcal{PT} inner product between $\phi_m(x)$ and $\phi_n(x)$ is $(-1)^n \delta_{mn} + \mathcal{O}(\epsilon^4)$.

We calculate the sum in (4) that represents $\mathcal{C}(x, y)$ by directly substituting the eigenfunctions $\phi_n(x)$ from (11) - (12). There are four regions of x and y to consider: (i) $x > \frac{\pi}{2}, y > \frac{\pi}{2}$; (ii) $x > \frac{\pi}{2}, y < \frac{\pi}{2}$; (iii) $x < \frac{\pi}{2}, y < \frac{\pi}{2}$; (iv) $x < \frac{\pi}{2}, y > \frac{\pi}{2}$. To zeroth-order in ϵ , ϕ_n is common to all four regions and the calculation is easy. We find that

$$\mathcal{C}^{(0)}(x, y) = \frac{2}{\pi} \sum_{n=0}^{\infty} (-1)^n \sin(n+1)x \sin(n+1)y. \quad (14)$$

This is just the Fourier sine series for the parity operator in the range $0 < x < \pi$:

$$\mathcal{C}^{(0)}(x, y) = \delta(x + y - \pi). \quad (15)$$

On the symmetric domain $-\frac{\pi}{2} < x < \frac{\pi}{2}$ this formula becomes $\mathcal{C}^{(0)}(x, y) = \delta(x + y)$, which is equivalent to the coordinate-space condition of completeness.

The calculation of $\mathcal{C}(x, y)$ to first order in ϵ requires the evaluation of Fourier sine and cosine series. These are expressed in terms of integrals of delta functions. The calculation is difficult and is described in detail in Ref. [7]. The result for the four regions can be condensed into a single expression:

$$\begin{aligned} \mathcal{C}^{(1)}(x, y) = & \frac{1}{4}i[x + y - \pi - \theta(\pi - x - y) (|x - y| - \pi) \\ & + \theta(x + y - \pi) (|x - y| - \pi)]. \end{aligned} \quad (16)$$

On the square symmetric region $-\frac{\pi}{2} < (x, y) < \frac{\pi}{2}$, this expression becomes

$$\mathcal{C}^{(1)}(x, y) = \frac{1}{4}i[x + y + \varepsilon(x + y) (|x - y| - \pi)], \quad (17)$$

where $\varepsilon(x)$ is the standard step function

$$\varepsilon(x) = \begin{cases} 1 & (x > 0), \\ 0 & (x = 0), \\ -1 & (x < 0). \end{cases} \quad (18)$$

Note that $\mathcal{C}^{(1)}(x, y)$ vanishes on the boundary of the square domain because the eigenfunctions $\phi_n(x)$ in (4) are required to vanish at $x = 0$ and $x = \pi$.

The procedure for calculating the second-order contribution $\mathcal{C}^{(2)}(x, y)$ to the \mathcal{C} operator is similar to but even more complicated than that used for calculating $\mathcal{C}^{(1)}(x, y)$. We must calculate sums of products of sines and cosines, but this time the presence of factors of $(n+1)^4$, $(n+1)^3$, and $(n+1)^2$ in the denominator requires the use of quadruple, triple, and double integrals of delta functions to simplify the expression for $\mathcal{C}^{(2)}(x, y)$. Combining the contributions from the four regions and transforming to the symmetric domain $-\frac{\pi}{2} < (x, y) < \frac{\pi}{2}$, we obtain the single expression:

$$\begin{aligned} \mathcal{C}^{(2)}(x, y) = & \frac{1}{96}\pi^3 + \frac{1}{8}xy\pi - \frac{1}{16}\pi^2(x + y) \varepsilon(x + y) + \frac{1}{8}\pi(x|x| + y|y|) \varepsilon(x + y) \\ & - \frac{1}{24}(x^3 + y^3) \varepsilon(x + y) - \frac{1}{24}(y^3 - x^3) \varepsilon(y - x) \\ & - \frac{1}{4}xy\{|x|[\theta(x - y) \theta(-x - y) + \theta(y - x) \theta(x + y)] \\ & + |y|[\theta(y - x) \theta(-x - y) + \theta(x - y) \theta(x + y)]\}. \end{aligned} \quad (19)$$

The function $\mathcal{C}^{(2)}(x, y)$ vanishes on the boundary of the symmetric square domain $-\frac{\pi}{2} < (x, y) < \frac{\pi}{2}$ because the eigenfunctions $\phi_n(x)$ from which it was constructed vanish at the boundaries of the square well.

In summary, our final result for the \mathcal{C} operator to order ϵ^2 on the symmetric domain $-\frac{\pi}{2} < (x, y) < \frac{\pi}{2}$ is

$$\mathcal{C}(x, y) = \delta(x + y) + \epsilon\mathcal{C}^{(1)}(x, y) + \epsilon^2\mathcal{C}^{(2)}(x, y) + \mathcal{O}(\epsilon^3), \quad (20)$$

where $\mathcal{C}^{(1)}(x, y)$ is given in (17) and $\mathcal{C}^{(2)}(x, y)$ is given in (19). We have verified by explicit calculation that to order ϵ^2 this \mathcal{C} operator obeys the algebraic equations (8). For example, in coordinate space the third of these equations, $\mathcal{C}^2 = 1$, reads

$$\int_{-\pi/2}^{\pi/2} dy \mathcal{C}(x, y) \mathcal{C}(y, z) = \delta(x - z) + \mathcal{O}(\epsilon^3). \quad (21)$$

The last step in this calculation is to determine the operator Q from (20) by using (9). This is a long calculation: We first multiply $\mathcal{C}(x, z)$ on the right by $\delta(z + y)$, the parity operator \mathcal{P} in coordinate space, and then integrate with respect to z . This gives the coordinate space representation of $\mathcal{C}\mathcal{P} = e^Q$. Next, we take the logarithm of the resulting expression and expand it as a series in powers of ϵ to obtain Q . We find that the coefficient of ϵ^2 in this expansion is zero, and we obtain a simple result for $Q(x, y)$ on the domain $-\frac{\pi}{2} < x < \frac{\pi}{2}$:

$$Q(x, y) = \frac{1}{4}i\epsilon[x - y + \varepsilon(x - y)(|x + y| - \pi)] + \mathcal{O}(\epsilon^3). \quad (22)$$

Thus, by expressing \mathcal{C} in the form $e^Q\mathcal{P}$, we have found that the operator Q for the \mathcal{PT} -symmetric square well model has an expansion in odd powers of ϵ , just as in the case of the cubic \mathcal{PT} -symmetric oscillator whose Hamiltonian is given in (7). Our result (22) for Q is an elementary function.

The most noteworthy property of the \mathcal{C} operator is that the Q operator in (22) is a nonpolynomial function, and such a structure had not been seen in previous studies of \mathcal{C} . We expected that for such a simple \mathcal{PT} -symmetric Hamiltonian it would be possible to calculate the \mathcal{C} operator exactly and in closed form. It surprised us that even for this elementary model the \mathcal{C} operator is so nontrivial.

4. Comparison of \mathcal{PT} -Symmetric and Hermitian Hamiltonians

Mostafazadeh has shown that the square root of the positive operator e^Q can be used to construct a similarity transformation that converts a non-Hermitian \mathcal{PT} -symmetric Hamiltonian H to an equivalent Hermitian Hamiltonian h [14]:

$$h = \rho^{-1}H\rho, \quad (23)$$

where the operator ρ is the square-root of $\mathcal{C}\mathcal{P}$: $\rho = e^{Q/2}$. The Hamiltonian h that results from the similarity transformation (23) has been studied perturbatively by Jones [15] and Mostafazadeh [16].

Equation (23) raises the following question: In which form of the quantum theory, the non-Hermitian or the Hermitian one, is it easier to perform calculations?

This question is answered in Ref. [8] where both forms of a non-Hermitian ix^3 quantum-mechanical Hamiltonian are compared. We summarize the argument here and demonstrate that it is much harder to perform calculations in the Hermitian theory because the perturbation series for the Hermitian Hamiltonian is constructed from divergent Feynman graphs. For the Hermitian version of the theory, dimensional continuation can be used to regulate the divergent graphs that contribute to the ground-state energy to order $\mathcal{O}(g^2)$. The results that are obtained are identical to those found more simply and without divergences in the non-Hermitian \mathcal{PT} -symmetric Hamiltonian. The $\mathcal{O}(g^4)$ contribution to the ground-state energy of the Hermitian version of the theory involves graphs with *overlapping divergences*, and such graphs are very difficult to regulate. In contrast, the graphs for the non-Hermitian version of the theory are finite to all orders and are easy to evaluate.

We focus here on the Hermitian Hamiltonian corresponding to the cubic non-Hermitian \mathcal{PT} -symmetric Hamiltonian

$$H = \frac{1}{2}p^2 + \frac{1}{2}x^2 + igx^3. \quad (24)$$

The eigenvalue problem corresponding to the quantum-mechanical Hamiltonian (24) is easy to solve perturbatively, and we can calculate the ground-state energy as a series in powers of g^2 . The fourth-order result is

$$E_0 = \frac{1}{2} + \frac{11}{8}g^2 - \frac{465}{32}g^4 + \mathcal{O}(g^6). \quad (25)$$

However, our objective is to study \mathcal{PT} -symmetric quantum field theories, and therefore we need to use Feynman-diagrammatic methods. For a quantum field theory the perturbation expansion of the ground-state energy is the negative sum of the connected Feynman graphs having no external lines. To evaluate Feynman graphs we must first determine the Feynman rule from the Lagrangian. Thus, we begin by constructing the Lagrangian corresponding to the Hamiltonian H in (24):

$$L = \frac{1}{2}(p\dot{x} + \dot{x}p) - H. \quad (26)$$

Because the interaction term is local (it depends only on x and not on p), the formula for \dot{x} is simple: $\dot{x} = p$. Thus, we have

$$L = \frac{1}{2}\dot{x}^2 - \frac{1}{2}x^2 - igx^3. \quad (27)$$

From (27) we read off the Euclidean Feynman rules: The three-point vertex amplitude is $-6ig$. In coordinate space a line connecting vertices at x and y is represented by $\frac{1}{2}e^{-|x-y|}$ and in momentum space the line amplitude is $\frac{1}{p^2+1}$. These Feynman rules are illustrated in Fig. 11.

In order g^2 two connected graphs contribute to the ground-state energy, and these are shown in Fig. 12. The symmetry number for graph (a1) is $\frac{1}{8}$ and the symmetry number for graph (a2) is $\frac{1}{12}$. Both graphs have vertex factors of $-36g^2$. Evaluating the Feynman integrals for (a1) and (a2) gives $V/4$ and $V/12$, respectively, where $V = \int dx$ is the volume of coordinate space. Thus, the sum of the graph amplitudes is $-\frac{11}{8}g^2V$. The contribution to the ground-state energy is the negative of this amplitude divided by V : $E_2 = \frac{11}{8}g^2$, which easily reproduces the g^2 term in (25).

Since the energy levels of the Hermitian Hamiltonian h obtained by means of the similarity transformation (23) are identical to those of H , we will try to recalculate the g^2 term in the expansion of the ground-state energy in (25) using the Feynman rules obtained from the transformed Hamiltonian h . The first step in this calculation is to construct the operator Q , which is given in Ref. [11] as

$$Q = \left(-\frac{4}{3}p^3 - 2S_{1,2}\right)g + \left(\frac{128}{15}p^5 + \frac{40}{3}S_{3,2} + 8S_{1,4} - 12p\right)g^3 + \mathcal{O}(g^5), \quad (28)$$

where the symbol $S_{m,n}$ represents a totally symmetric combination of m factors of p and n factors of x .

We can use (23) to construct h . The result taken from Refs. [15, 16] is

$$h = \frac{1}{2}p^2 + \frac{1}{2}x^2 + \left(\frac{3}{2}x^4 + 3S_{2,2} - \frac{1}{2}\right)g^2 + \left(-\frac{7}{2}x^6 - \frac{51}{2}S_{2,4} - 36S_{4,2} + 2p^6 + \frac{15}{2}x^2 + 27p^2\right)g^4 + \mathcal{O}(g^6). \quad (29)$$

To obtain the Feynman rules we construct the corresponding Hermitian Lagrangian ℓ . To do so, we must replace the operator p with the operator \dot{x} by using the formula $p = \dot{x} - 6g^2s_{1,2}$, where $s_{m,n}$ represents a totally symmetric combination of m factors of \dot{x} and n factors of x . The result for the Hermitian Lagrangian ℓ is

$$\ell = \frac{1}{2}\dot{x}^2 - \frac{1}{2}x^2 - \left(\frac{3}{2}x^4 + 3s_{2,2} - \frac{1}{2}\right)g^2$$

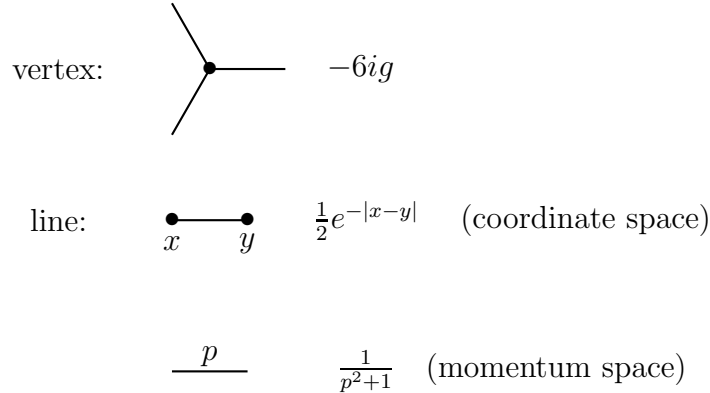


Figure 11. Feynman rules for the Lagrangian (27). For this simple local trilinear interaction the Feynman graphs are built from three-point vertices connected with lines. The line amplitudes in both coordinate space and momentum space are shown.

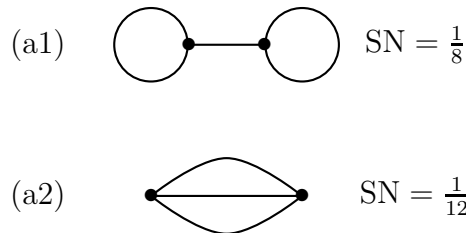


Figure 12. The two connected vacuum graphs, labeled (a1) and (a2), contributing to the ground-state energy of H in (24) to order g^2 . The symmetry numbers for each graph are indicated.

$$+ \left(\frac{7}{2}x^6 + \frac{87}{2}s_{2,4} + 36s_{4,2} - 2\dot{x}^6 - \frac{27}{2}\dot{x}^2 - 27\dot{x}^2 \right) g^4 + \mathcal{O}(g^6). \quad (30)$$

From this Lagrangian we read off the Euclidean-space Feynman rules. Unlike the \mathcal{PT} version of the theory, increasingly many new vertices appear in every order of perturbation theory. The three vertices to order g^2 are shown in Fig. 13 and the six vertices to order g^4 are shown in Fig. 14. Some of the lines emerging from the vertices have tick marks to indicate a derivative in coordinate space and a factor of ip in momentum space. The tick marks are a result of the *derivative* coupling terms in the Lagrangian ℓ . This derivative coupling gives rise to divergent Feynman graphs.

We now use the Feynman rules in Fig. 13 to construct the vacuum graphs contributing to the ground-state energy in order g^2 . These graphs are shown in Fig. 15. The simplest graph is (b3) because there is no Feynman integral to perform. This graph

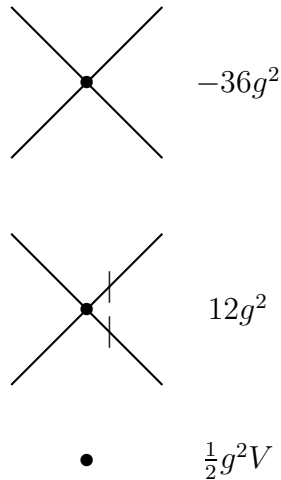


Figure 13. The three Euclidean-space vertices to order g^2 for the Hermitian Lagrangian ℓ in (30). Note that the second vertex has tick marks on two of the legs. These tick marks indicate coordinate-space derivatives that arise because of derivative coupling. Derivative coupling results in divergent Feynman graphs.

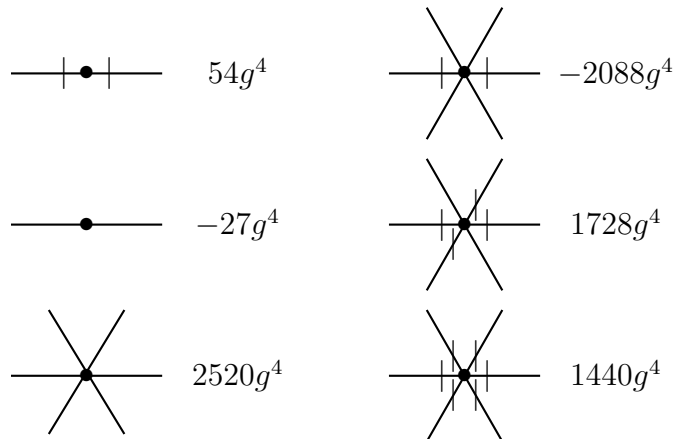


Figure 14. The six Euclidean-space vertices to order g^4 for the Hermitian Lagrangian ℓ in (30). Four of the vertices have tick marks on the legs to indicate derivative coupling.

arises from the constant term in ℓ in (30). The value of this graph is $\frac{1}{2}g^2V$.

Graph (b1) has symmetry number $\frac{1}{8}$ and vertex factor $-36g^2$ and the Feynman integral in momentum space is

$$\left(\int_{-\infty}^{\infty} \frac{dp}{2\pi} \frac{1}{p^2 + 1} \right)^2 = \frac{1}{4}. \quad (31)$$

The integrals associated with this graph are convergent. The value of graph (b1) is $-\frac{9}{8}g^2V$, where the factor of V comes from the translation invariance of the graph.

The interesting graph is (b2). The symmetry number is $\frac{1}{4}$, the vertex factor is $12g^2$, and the Feynman integral in momentum space is

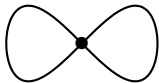
$$\int_{-\infty}^{\infty} \frac{dp}{2\pi} \frac{p^2}{p^2 + 1} \int_{-\infty}^{\infty} \frac{dq}{2\pi} \frac{1}{q^2 + 1}. \quad (32)$$

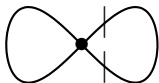
The q integral is convergent and gives the value $\frac{1}{2}$. However, the p integral is divergent. We therefore regulate it using dimensional continuation and represent its value as the limit as the number of dimensions approaches 1:

$$\lim_{D \rightarrow 1} 2 \int_0^{\infty} \frac{r^{D-1} dr}{2\pi} \frac{r^2}{r^2 + 1} = \lim_{D \rightarrow 1} \frac{\Gamma(1 + \frac{1}{2}D) \Gamma(-\frac{1}{2}D)}{2\pi} = -\frac{1}{2}. \quad (33)$$

Hence, the value of graph (b2) is $-\frac{3}{4}g^2V$, where again the volume factor V comes from translation invariance. Adding the three graphs (b1), (b2), and (b3), dividing by V , and changing the sign gives the result $\frac{11}{8}g^2$, which reproduces the result in (25). This calculation is more difficult than that using the Feynman rules in Fig. 1 because there is a divergent graph. It is surprising to find a divergent graph in one-dimensional quantum field theory (quantum mechanics). This infinite graph is not associated with a renormalization of a physical parameter in the Lagrangian. Rather, it is an artifact of the derivative coupling terms that arise from the similarity transformation (23).

This dimensional-continuation procedure is effective because it extracts the correct finite contribution from each of the divergent graphs. However, this procedure is much more difficult to apply when there are graphs having overlapping divergences, as we

(b1)  SN = $\frac{1}{8}$

(b2)  SN = $\frac{1}{4}$

(b3)  SN = 1

Figure 15. The three graphs contributing to the ground-state energy of the Hermitian Lagrangian ℓ in (30) in order g^2 . While graphs (b1) and (b3) are finite, the Feynman integral for graph (b2) diverges and must be regulated to obtain a finite result.

will now demonstrate. Let us extend the calculation of the ground-state energy to next order in powers of g^2 . This calculation is straightforward in the non-Hermitian theory, while it is nearly impossible in the Hermitian theory. The difficulty is not just due to the arithmetic difficulty of sorting through large numbers of graphs, but rather is one of principle. The problem is that there are two graphs having overlapping divergences, and calculating the numerical values of the corresponding regulated graphs remains an unsolved problem, even in one-dimensional field theory (quantum mechanics)!

There are five graphs (f1) – (f5) contributing in order g^4 to the ground-state energy of the non-Hermitian Hamiltonian H in (24). These are shown in Fig. 16. The symmetry numbers for these graphs are indicated in the figure. The vertex factors for all these graphs are $1296g^4$. The Feynman integrals for these graphs are $\frac{1}{16}V$ for (f1), $\frac{11}{864}V$ for (fx2), $\frac{1}{8}V$ for (f3), $\frac{1}{36}V$ for (fx4), and $\frac{1}{96}V$ for (f5). Thus, the sum of the graphs is $\frac{465}{32}V$. The negative of this amplitude divided by V is $E_4 = -\frac{465}{32}g^4$. This reproduces the order g^4 term in the perturbation expansion for the ground-state energy in (25).

There are seventeen graphs of order g^4 contributing to the ground-state energy of the Hermitian Hamiltonian (29). These graphs, along with their symmetry numbers, are shown in Fig. 17. Seven of these graphs, (g1), (g3), (g7), (g8), (g10), (g11), and (g16) are finite and easy to calculate. The Feynman integrals for the remaining graphs are infinite and must be regulated. Dimensional continuation can be readily implemented as in (33) except for the graphs (g15) and (g17). These two graphs are difficult to regulate

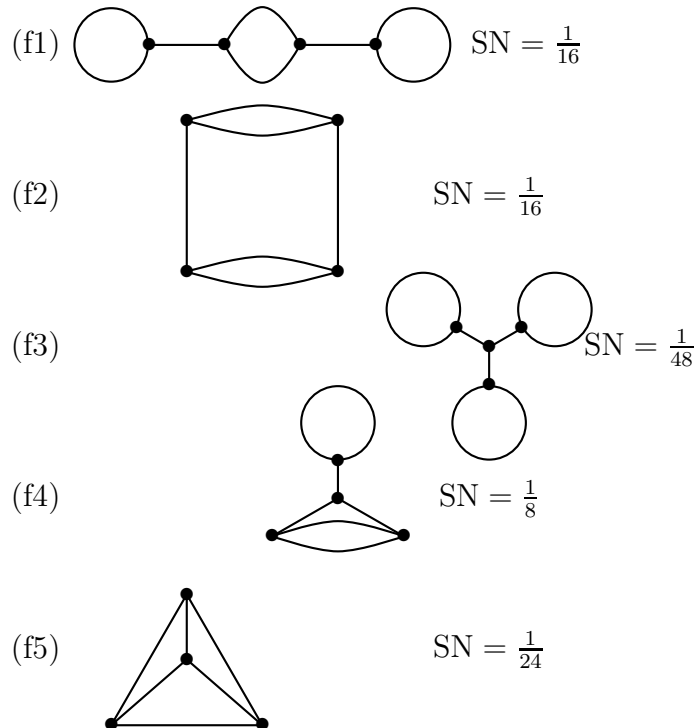


Figure 16. The five vacuum graphs contributing to the ground-state energy of the non-Hermitian \mathcal{PT} -symmetric Hamiltonian H in (24) to order g^4 . These graphs are all finite and very easy to evaluate.

because they have overlapping divergences. It is dismaying to find Feynman graphs having overlapping divergences in one-dimensional quantum field theory! Since the g^4 contribution to the ground-state energy is given in (25), we deduce that the sum of the regulated values of these two graphs (multiplied by their respective symmetry numbers and vertex factors) must be $\frac{21}{16}g^4V$. There is no easy way to obtain this result.

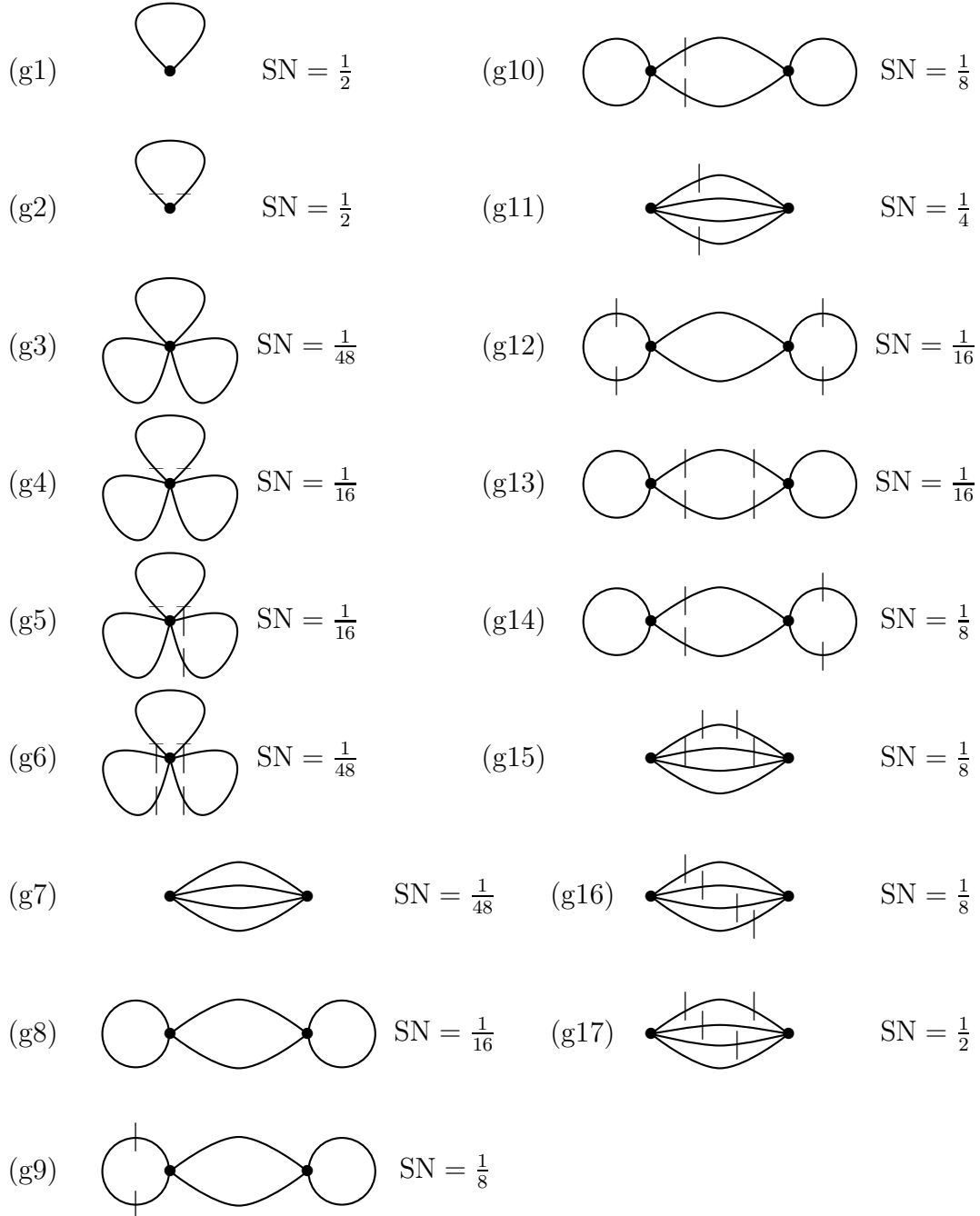


Figure 17. The seventeen graphs contributing to the order g^4 term in the perturbation expansion for the ground-state energy of the Hermitian Hamiltonian h in (29). Ten of these graphs have divergent Feynman integrals. Of these ten, eight are relatively easy to regulate using dimensional continuation. However, graphs (g15) and (g17) have overlapping divergences, and are therefore extremely hard to evaluate.

This study was motivated by the concern that solving problems in quantum field theory might be difficult in non-Hermitian theories. The usual techniques rely on the Schwinger action principle, the construction of functional integrals, and the identification and application of Feynman rules. These procedures are usually formulated in a Hermitian setting. The good news is that these standard techniques work perfectly in a non-Hermitian context, but the bad news is that they are difficult to apply if the non-Hermitian theory is first transformed to the equivalent Hermitian one.

We conclude by citing the comment of Jones in the second paper in Ref. [15] regarding the critique of \mathcal{PT} -symmetric theories in Ref. [17]: “Clearly, this [Eq. (29)] is not a Hamiltonian that one would have contemplated in its own regard were it not derived from [Eq. (24)]. It is for this reason that we disagree with the contention of Mostafazadeh [17] that, ‘A consistent probabilistic \mathcal{PT} -symmetric quantum theory is doomed to reduce to ordinary quantum mechanics.’” Mostafazadeh appears to be correct in arguing that a \mathcal{PT} -symmetric theory can be transformed to a Hermitian theory by means of a similarity transformation. However, we have shown that the difficulties with the Hermitian theory are severe and virtually insurmountable because this theory possesses a Feynman perturbation expansion that becomes increasingly divergent as one goes to higher order. The divergences are not removable by renormalization. Rather, they are due to increasingly singular derivative interactions. In contrast, the non-Hermitian \mathcal{PT} -symmetric theory is free from all such difficulties.

5. Reflectionless Potentials

Normally, to find the eigenvalues of a \mathcal{PT} -symmetric Hamiltonian one must impose boundary conditions inside of a pair of wedges in the complex plane. However, for a special class of such \mathcal{PT} quantum mechanical Hamiltonians it is possible to impose the \mathcal{PT} -symmetric boundary conditions on the real axis, which lies on the edges of the complex wedges. This allows us to obtain the \mathcal{PT} -symmetric spectrum by imposing the requirement that the potential be reflectionless. It further allows us to formulate some conjectures regarding the possible applicability of \mathcal{PT} -symmetric quantum mechanics to problems in cosmology [9].

Consider the class of Hamiltonian the Schrödinger equations

$$-\psi_n''(x) + [x^{2K}(ix)^\epsilon - E_n]\psi_n(x) = 0, \quad (34)$$

where the eigenfunction $\psi_n(x)$ satisfies the \mathcal{PT} -symmetric boundary conditions that $\psi_n(x)$ vanishes as $|x| \rightarrow \infty$ in two wedges placed symmetrically about the imaginary axis in the lower-half x plane. These wedges are determined by analytic continuation of the leading-order exponentials in the asymptotic solutions of (34), namely

$$\psi(x) \sim \exp\left(\pm \frac{i^{\epsilon/2} x^{K+1+\epsilon/2}}{K+1+\epsilon/2}\right). \quad (35)$$

Within each wedge, one of the two solutions decays and one grows. The wedges are

centered about the asymptotic directions

$$\theta_{\text{right}} = -\frac{\epsilon\pi}{4K+2\epsilon+4}, \quad \theta_{\text{left}} = -\pi + \frac{\epsilon\pi}{4K+2\epsilon+4}. \quad (36)$$

The exponents in these asymptotic exponentials are purely real on the Stokes lines at the centers of the wedges. It is easy to check that

$$\begin{aligned} &\text{in the right wedge: } \psi_- \text{ decays and } \psi_+ \text{ grows;} \\ &\text{in the left wedge: } \begin{cases} \psi_- \text{ decays and } \psi_+ \text{ grows if } K \text{ is odd,} \\ \psi_+ \text{ decays and } \psi_- \text{ grows if } K \text{ is even.} \end{cases} \end{aligned} \quad (37)$$

The opening angle of each wedge is $\theta_{\text{opening angle}} = \frac{2\pi}{2K+\epsilon+2}$. The wedge boundaries are anti-Stokes lines, where the solutions are purely oscillatory [2].

We are concerned here with the infinite subclass $\epsilon = 2$ for which the potential in (1), that is

$$V(x) = -x^{2K+2} \quad (K = 1, 2, 3, \dots), \quad (38)$$

is real and appears to have the wrong sign to possess bound states. However, the \mathcal{PT} -symmetric solution to the Schrödinger equation (34) with the complex boundary conditions described above does have bound states. (The potential $-x^2$ is not included in this subclass.)

When $\epsilon = 2$, the upper edges of the right and left wedges, where the solutions are purely oscillatory, lie exactly along the positive and negative real- x axis. On the real axis the potential (38), when interpreted in conventional terms, describes one-dimensional scattering solutions of the Schrödinger equation, that is, traveling waves rather than decaying exponentials at infinity. As far as the energy spectrum is concerned, we may replace the non-Hermitian eigenvalue problem in the complex wedges by a conventional Hermitian problem defined by the requirement that the potential be reflectionless. (To be precise, we do *not* claim that these two quantum theories, the non-Hermitian \mathcal{PT} -symmetric theory defined in the complex wedges and the Hermitian theory defined on the real axis, are the same. However, these two distinct theories do have the same energy spectrum and eigenfunctions.

To justify replacing the \mathcal{PT} -symmetric theory by the Hermitian one, consider the two dominant exponentials (35) when $\epsilon = 2$:

$$\psi_{\pm}(x) \sim \exp\left(\pm i \frac{x^{K+2}}{K+2}\right) \quad (K = 1, 2, 3, \dots). \quad (39)$$

For real x these behaviors represent waves traveling in directions given by the sign of the current $\text{Im}(\psi_{\pm}^* \psi'_{\pm})$, which is proportional to $\pm x^{K+1}$. Thus,

when $x > 0$:

$\psi_+(x)$ travels to the right and $\psi_-(x)$ travels to the left;

when $x < 0$:

$$\begin{cases} \psi_+(x) \text{ travels to the right and } \psi_-(x) \text{ travels to the left } (K \text{ odd}), \\ \psi_-(x) \text{ travels to the right and } \psi_+(x) \text{ travels to the left } (K \text{ even}). \end{cases} \quad (40)$$

These conditions match those for decay and growth in (37), so decay in the non-Hermitian problem corresponds to a purely left-going wave that is reflectionless in the corresponding conventional Hermitian problem. Under \mathcal{PT} reflection [replacing $x \rightarrow -x$ and $i \rightarrow -i$ in (39)], both wave directions reverse if K is even and do not reverse if K is odd. Reflectionlessness persists in both cases.

The corresponding energies can be approximated by the WKB method, starting with identification of the two turning points, defined by $V(x) = E$, in the wedges described above. The turning points are

$$x_{\text{right}} = E^{1/(2K+2)} e^{-i\pi/(2K+2)} \quad \text{and} \quad x_{\text{left}} = E^{1/(2K+2)} e^{-i\pi+i\pi/(2K+2)}. \quad (41)$$

Quantization according to $\int_{x_{\text{left}}}^{x_{\text{right}}} dt \sqrt{E - V(t)} = (n + \frac{1}{2}) \pi$ for large n [18] gives

$$E_n \sim \left(\frac{(n + 1/2) \sqrt{\pi} (K + 2) \Gamma[(K + 2)/(2K + 2)]}{\Gamma[1/(2K + 2)] \cos[\pi/(2K + 2)]} \right)^{(2K+2)/(K+2)} \quad (42)$$

for $K = 1, 2, 3, \dots$. Reflectionlessness can be regarded as the consequence of destructive interference between exponentially small waves reflected separately from the turning points x_{right} and x_{left} in (41).

Thus, we have shown that for an infinite class of non-Hermitian \mathcal{PT} -symmetric Hamiltonians having unbroken \mathcal{PT} symmetry, and hence real positive discrete spectra, there is a corresponding set of Hermitian Hamiltonians whose spectra and eigenfunctions become identical when the condition of reflectionlessness is imposed. Although these pairs of Hamiltonians do not describe the same physics because the inner product needed to calculate matrix elements is different, this intriguing association between non-Hermitian and Hermitian Hamiltonians helps to explain the surprising observation [2] that the spectra of some non-Hermitian Hamiltonians can be real.

The connection between reflectionless potentials and \mathcal{PT} symmetry may be useful in quantum cosmology. Recently, much attention has been given to Anti-de Sitter cosmologies [19] and de Sitter cosmologies [20, 21]. In the AdS description the universe propagates reflectionlessly in the presence of a wrong-sign potential ($-x^6$, for example). In the dS case the usual Hermitian quantum mechanics is abandoned and replaced by a non-Hermitian one in which there are ‘meta-observables’. The non-Hermitian inner product that is used in the dS case is based on the \mathcal{CPT} theorem just as the \mathcal{CPT} inner product is used in \mathcal{PT} -symmetric quantum theory [4].

Acknowledgments

I thank the US Department of Energy for financial support.

References

- [1] C. M. Bender, J. Chen, D. W. Darg, and K. A. Milton, arXiv: math-ph/XXXXXXXXXX; D. W. Darg, M.Sc. Thesis, Imperial College, London (2005, unpublished).
- [2] C. M. Bender and S. Boettcher, Phys. Rev. Lett. **80**, 5243 (1998).

- [3] P. Dorey, C. Dunning, and R. Tateo, *J. Phys. A: Math. Gen.* **34**, L391 (2001) and **34**, 5679 (2001).
- [4] C. M. Bender, D. C. Brody, and H. F. Jones, *Phys. Rev. Lett.* **89**, 270401 (2002).
- [5] C. M. Bender, S. Boettcher, and P. N. Meisinger, *J. Math. Phys.* **40**, 2201 (1999).
- [6] A. Nanayakkara, *Czech. J. Phys.* **54**, 101 (2004) and *J. Phys. A: Math. Gen.* **37**, 4321 (2004).
- [7] C. M. Bender and B. Tan, *J. Phys. A: Math. Gen.* (to be published) [arXiv: quant-ph/0601123]; B. Tan, M.Sc. Thesis, Imperial College, London (2005, unpublished).
- [8] C. M. Bender, J. Chen, and K. A. Milton, *J. Phys. A: Math. Gen.* **39**, 1657-1668 (2006) [arXiv: hep-th/0511229].
- [9] Z. Ahmed, C. M. Bender, and M. A. Berry, *J. Phys. A: Math. Gen.* **38**, L627-L630 (2005) [arXiv:quant-ph/0508117].
- [10] M. Znojil, *Phys. Lett. A* **285**, 7 (2001).
- [11] M. Znojil and G. Lévai, *Mod. Phys. Lett. A* **16**, 2273 (2001); B. Bagchi, S. Mallik, and C. Quesne, *Mod. Phys. Lett. A* **17**, 1651 (2002); A. Mostafazadeh and A. Batal, *J. Phys. A: Math. Gen.* **37**, 11645 (2004); M. Znojil, *J. Math. Phys.* **46**, 062109 (2005) and arXiv: quant-ph/0511085.
- [12] C. M. Bender, P. N. Meisinger, and Q. Wang, *J. Phys. A: Math. Gen.* **36**, 1973 (2003); C. M. Bender, J. Brod, A. Refig, and M. E. Reuter, *J. Phys. A: Math. Gen.* **37**, 10139 (2004).
- [13] C. M. Bender, D. C. Brody, and H. F. Jones, *Phys. Rev. Lett.* **93**, 251601 (2004) and *Phys. Rev. D* **70**, 025001 (2004).
- [14] A. Mostafazadeh, *J. Math. Phys.* **33**, 205 (2002) and *J. Phys. A: Math. Gen.* **36**, 7081 (2003).
- [15] H. F. Jones, *Czech. J. Phys.* **54**, 1107 (2004); *J. Phys. A: Math. Gen.* **38**, 1741 (2005).
- [16] A. Mostafazadeh, *J. Phys. A: Math. Gen.* **38**, 6557 (2005) and Erratum **38**, 8185 (2005).
- [17] A. Mostafazadeh, arXiv:quant-ph/0310164.
- [18] M. V. Berry and K. E. Mount, *Reps. Prog. Phys.* **35**, 315-397 (1972).
- [19] T. Hertog and G. T. Horowitz, *JHEP* **04**, 005 (2005).
- [20] E. Witten, arXiv:hep-th/016109.
- [21] R. Bousso, A. Maloney, and A. Strominger, *Phys. Rev. D* **65**, 104039 (2002).